Supporting Information

Chemical Mechanism and Tunability of Surface-enhanced Raman Scattering of Pyridine on Heteronuclear Coinage Metal Diatomic Clusters: A Density Functional Study

Lei Chen, [†, ‡,⊥] Zhengqiang Li, [†] Yan Meng, [‡,∥] Ming Lu, [†] Zhigang Wang, [*,‡,∥] and Rui-Qin Zhang, [*,⊥,∥]

[†]Key Laboratory for Molecular Enzymology and Engineering of Ministry of Education, College of Life Sciences, Jilin University, Changchun, 130012, China

[‡]Institute of Atomic and Molecular Physics, Jilin University, Changchun 130012, China

[⊥]Department of Physics and Materials Science and Centre for Functional Photonics (CFP), City University of Hong Kong, Hong Kong SAR, China

[∥]Beijing Computational Science Research Center, Beijing 100084, P. R. China

Supporting Information

Supporting Information for the paper entitled "Chemical Mechanism and Tunability of Surface-enhanced Raman Scattering of Pyridine on Heteronuclear Coinage Metal Diatomic Clusters: A Density Functional Study" by Lei Chen, Zhengqiang Li, Yan Meng, Ming Lu, Zhigang Wang, and Rui-Qin Zhang.

1. Optimized geometrical parameters of the pyridine and its adsorption state on various HCMDCs.
2. Molecular orbital analysis and band gap analysis of the HCMDC-Py complexes.
3. Static Raman vibrational analysis of the pyridine interacting with different HCMDCs.
4. Raman vibrational analysis of the HCMDC-Py complexes at 785 nm, 514 nm, and 488 nm excitation wavelengths.
5. The complete author list of reference 23.

1. Optimized geometrical parameters.

Table S1. Geometrical parameters of the pyridine molecule and HCMDC-Py complexes optimized at the B3LYP/6-311+G(d, p) (C, N, H) /ECP-Lanl2DZ (M) level (bond length in angstrom, bond angle in degrees).

	pyridine	Cu_2-Py	Ag-Cu-Py	Au-Cu-Py	Cu-Ag-Py	Ag_2-Py	Au-Ag-Py	Cu-Au-Py	Ag-Au-Py	Au_2-Py
N-C1	1.337	1.344	1.344	1.346	1.340	1.341	1.343	1.340	1.341	1.344
C1-C2	1.394	1.389	1.389	1.389	1.391	1.391	1.390	1.391	1.390	1.389
C2-C3	1.392	1.392	1.392	1.392	1.392	1.392	1.391	1.392	1.392	1.392
C1-H	1.086	1.084	1.084	1.083	1.085	1.084	1.084	1.084	1.084	1.082
C2-H	1.084	1.083	1.083	1.083	1.083	1.083	1.083	1.083	1.083	1.083
C3-H	1.084	1.083	1.084	1.084	1.084	1.084	1.084	1.084	1.084	1.084
M1-M2		2.286	2.445	2.412	2.439	2.616	2.595	2.411	2.600	2.568
A(1,11,5)	117.2	118.2	118.2	118.2	118.2	118.2	118.2	118.6	118.6	118.6
A(2,1,6)	120.3	121.2	121.2	121.2	121	121	121	121.4	121.4	121.5
A(2,1,11)	123.6	122.7	122.7	122.6	122.8	122.8	122.7	122.6	122.5	122.4
A(6,1,11)	116	116.1	116.1	116.2	116.2	116.2	116.3	116.1	116.1	116.2
A(1,2,3)	118.5	118.9	118.9	118.9	118.7	118.7	118.8	118.8	118.8	119
A(1,2,7)	120.2	119.8	119.8	119.7	120	120	119.8	119.9	119.8	119.6
A(3,2,7)	121.3	121.4	121.4	121.4	121.4	121.4	121.4	121.4	121.4	121
A(2,3,4)	118.5	118.6	118.7	118.7	118.7	118.7	118.7	118.7	118.7	118.6

A(2,3,8)	120.7	120.7	120.7	120.7	120.7	120.6	120.6	120.6	120.6	120.7
A(4,3,8)	120.7	120.7	120.7	120.7	120.7	120.6	120.6	120.6	120.6	120.7

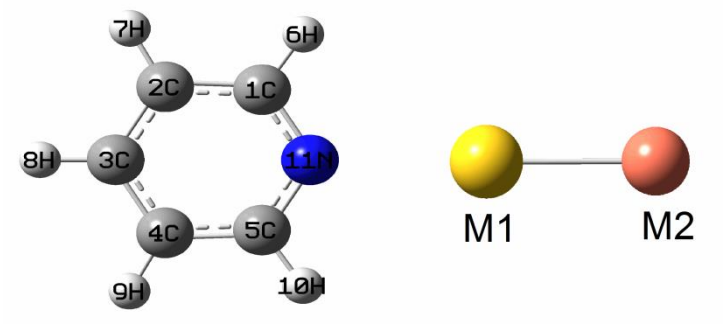

Figure S1. Schematic diagram of the pyridine molecule adsorbed on the HCMDC.

The changes of structural parameter in the pyridine molecule are closely related to the binding site and the composition of the HCMDC. The variation is quite similar to that of a molecule interacting with a single coinage metal cluster. Table S1 shows that the change in pyridine is no more than 0.01 Å for bond lengths and 1^{o} for bond angles. The structural parameters of the pyridine molecule change evidently, especially in the region close to the HCMDC.

The calculated bond distances between the N atom and the adjacent coinage metal atom in the HCMDC-Py complexes are presented in Table 1; the bonding energy and charge transferred from the pyridine to HCMDC are also listed in this table. Fig. 1 presents the charge distribution on metal atoms of HCMDC before and after the adsorption of the pyridine molecule. In all configurations, the Au atom of Au-Cu-Py carrying -0.510 e shows the largest negative electrical characteristics and the Cu atom carrying 0.461 e shows the largest positive electrical characteristics. In order to make a direct comparison with the interaction between pyridine molecule and a single coinage metal, we repeated Wu's study of the bond natures of Py-M_2 complexes (M=Cu, Ag, Au) and present the data in Table 1.[23] From the data in Table 1, we can draw the following conclusions: In contrast to other two HCMDCs, the Au-Cu HCMDC shows the largest property change when the pyridine molecule is adsorbed on its two ends, with an energy difference of 18.67 kcal/mol and charge transfer difference of 0.022 e. Among the interactions of pyridine adsorbed on the Cu-Au

HCMDC and those of the pyridine binding to the Cu_2 and Au_2 single metal clusters, the binding energy order is Au-Cu-Py＞Au_2-Py＞Cu_2-Py＞Cu-Au-Py, the charge transfer order is Au_2-Py＞Cu-Au-Py＞Au-Cu-Py＞Cu_2-Py, and the R(N-M) order is Cu-Au-Py＞Au_2-Py＞Cu_2-Py＞Au-Cu-Py.

For the Au-Ag HCMDC, the binding energy of the Au-Ag-Py (Ag-Au-Py) is 18.91 Kcal/mol (11.44 Kcal/mol) and the energy difference is the smallest among the three HCMDCs. In contrast to the properties of the pyridine adsorbed on Au_2 and Ag_2, the trend is Au_2-Py＞Au-Ag-Py＞Ag-Au-Py＞Ag_2-Py for the binding energy, Au_2-Py＞Ag-Au-Py ＞Au-Ag-Py＞Ag_2-Py for the charge transfer, and Ag_2-Py＞Au-Ag-Py＞Ag-Au-Py＞Au_2-Py for the bond length of N-M. Comparing the interactions between pyridine and Cu-Ag HCMDC with those of pyridine with Cu_2 and Ag_2 single coinage metal clusters, we find that the charge transfer from the pyridine molecule to the metal cluster (Q (pyridine→M)) is in an order of Ag_2-Py＞Cu-Ag-Py＞Ag-Cu-Py＞Cu_2-Py, the bond length between N and coinage metal atoms is in an order of Cu-Ag-Py＞Ag_2-Py＞Cu_2-Py＞Ag-Cu-Py, and the binding energy is in an order of Ag-Cu-Py＞Cu_2-Py＞Cu-Ag-Py＞Ag_2-Py. The binding energy of the Ag-Cu-Py is significantly stronger than that of the Cu-Ag-Py, but there is little difference in bonding natures between the Ag-Cu-Py and Cu_2-Py configurations and between the Cu-Ag-Py and Ag_2-Py complexes. Among all of the nine complexes except for the Cu_2-Py and Au_2-Py configurations, the Au-Cu-Py has the strongest interaction with the biggest binding energy and the smallest R (N-M) bond length at the ground state.

NBO analysis shows that the natural charge redistribution depends on compositions of metal cluster and adsorption site. Compared to the binding nature between the pyridine molecule and a single coinage metal cluster, the HCMDC can obviously lead to changes in binding energy, charge transfer, and bond length. Among different adsorption sites of the pyridine on the HCMDC, there are many significant differences in binding energy, charge transfer, and bond length between N and the coinage metal atoms. The bonding interaction is sensitive to binding site.

2. Molecular orbital analysis and band gap analysis.

Table S2. The calculated band gaps (in eV) of different HCMDC-Py complexes.

Model	Ag-Cu-Py	Cu-Ag-Py	Cu-Au-Py	Au-Cu-Py	Au-Ag-Py	Ag-Au-Py	Py
LUMO	-2.14	-1.92	-1.83	-2.38	-2.29	-1.89	-1.14
HOMO	-4.50	-4.62	-5.17	-5.31	-5.35	-5.17	-7.23
gap	2.36	2.70	3.34	2.93	3.06	3.28	6.09

Comparing the band gap of the pyridine molecule with that of the HCMDC-Py, we find that the transition energies from HOMO to LUMO of the HCMDC-Py are much lower than that of the pyridine molecule, and this case is similar to that of a pyridine interacting with a single coinage metal cluster. The band gaps of pyridine molecule adsorbed on the HCMDC change with the different adsorption sites. Band gap analysis suggests that the difference between the two complexes of Au-Cu and Ag-Cu interacting with the pyridine molecule is about 0.4 eV, while the value is 0.22 eV for the Au-Ag HCMDC. The band gap is 2.36 eV for the Ag-Cu-Py and 2.70 for the Cu-Ag-Py. Together with 2.63 eV for the Cu_2-Py and 2.93 eV for the Ag_2-Py, band gaps form the following sequence: Ag_2-Py＞Cu-Ag-Py＞Cu_2-Py＞Ag-Cu-Py. Performing the same band gap analysis for the pyridine molecule binding to other HCMDCs and to the corresponding single metal clusters, we obtained the following band gap sequences: Au_2-Py ＞ Cu-Au-Py ＞ Au-Cu-Py ＞ Cu_2-Py for the pyridine molecule adsorbed on the Au-Cu HCMDC, and Au_2-Py＞Ag-Au-Py＞Au-Ag-Py＞Ag_2-Py for the pyridine molecule adsorbed on the Ag-Au HCMDC.

In order to analyze the SERS chemical mechanism of the HCMDC-Py complexes, we calculated the three lowest singlet excited states using time-dependent density-functional theory (TD-DFT), which is an efficient method of obtaining a physical understanding of excitation process. Table 2 not only lists the transition energies and oscillator strengths for the three lowest singlet excited states in six stable HCMDC-Py complexes but also presents the characteristic charge transfer transitions according to

each excited state. Compared to these transition energies of the pyridine with single coinage metal complexes for the S_1 excited state (1.79 eV for Cu_2-Py, 2.09 eV for Ag_2-Py, 2.87 eV for Au_2-Py), we find that the transition energies for the S_1 excited states change evidently. For the two complexes consisting of the Cu-Au HCMDC and the pyridine molecule, the transition energy for S_1 is found to be 2.74 eV for the Cu-Au-Py and 2.36 eV for the Au-Cu-Py. The pyridine molecule adsorbed on different adsorption sites of the HCMDC can result in significant changes in transition energy according to different excited states.

In order to understand the interaction characteristics between pyridine molecule and HCMDC, we analyzed the molecular orbital of the HCMDC-Py complexes. Figs. 6 and 7 present the calculated molecular orbital energy levels and shapes (HOMO, HOMO-1, HOMO-2, LUMO, LUMO+1, LUMO+2) of the HCMDC-Py complexes. From Fig. 7, we find that the densities of HOMO, HOMO-1, and HOMO-2 of all HCMDC-Py structures are almost totally distributed on the metal cluster, while there are many differences in LUMO, LUMO+1, and LUMO+2. It is very interesting that the change of the adsorption sites of the same HCMDC can change the order of the unoccupied electronic orbitals. For the two configurations of the Au-Cu HCMDC interacting with the pyridine molecule, the LUMO and LUMO+1 of the Au-Cu-Py are mainly distributed on the pyridine molecule and the LUMO+2 is mainly confined in the HCMDC. However, for the Cu-Au-Py, the LUMO and LUMO+2 are mainly distributed on the pyridine molecule and the LUMO+1 is confined in the Au-Cu HCMDC. The order of LUMO+1 and LUMO+2 of the above two complexes is reversed. These MO distribution differences can lead to changes of the low-lying excited states for the two structures of the pyridine interacting with the Au-Cu HCMDC.

The distribution of LUMO, LUMO+1, and LUMO+2 of the Ag-Cu-Py is similar to that of the Cu-Ag-Py. The LUMO and LUMO+1 are mainly distributed on the pyridine molecule, and LUMO+2 orbitals are all limited to region of the metal cluster. With regard to the Au-Ag-Py and Ag-Au-Py complexes, the LUMO and LUMO+1 of

the former are mainly located on the pyridine molecule and LUMO+2 is mainly limited to the region of the HCMDC, similar to the Ag-Cu-Py, Cu-Ag-Py, and Au-Cu-Py. However, the LUMO and LUMO+2 of Ag-Au-Py complex are mainly distributed on the pyridine molecule, and the LUMO+1 is mainly limited to the region of the HCMDC.

3. Static Raman vibrational analysis.

Table S3. Calculated static Raman scattering peak positions (wave number in cm^{-1}) and differential Raman scattering cross section (DRCS in units of $10^{-30}cm^2/sr$) of selected totally symmetric modes of the HCMDC-Py complexes under a C_{2v} point group using the B3LYP method.

	υ_{6a}		υ_1		υ_{12}		υ_{9a}		υ_{8a}	
	peak	dσ/dΩ	peak	dσ/dΩ	peak	dσ/dΩ	peak	dσ/dΩ	peak	dσ/dΩ
pyridine	597	0.2	978	1.4	1014	1.6	1202	0.4	1573	0.7
Ag-Au-Py	613	0.1	991	3.0	1016	2.6	1196	0.5	1584	2
Au-Ag-Py	619	0.1	996	2.2	1021	1.3	1204	0.3	1590	1.1
Cu-Ag-Py	615	0.1	993	2.2	1017	1.6	1201	0.04	1585	1.2
Ag-Cu-Py	628	0.5	998	5.6	1023	0.4	1199	0.7	1590	6.4
Au-Cu-Py	635	0.6	1001	6.2	1028	0.1	1201	0.8	1592	6.2
Cu-Au-Py	613	0.2	991	3.5	1016	2.2	1196	0.6	1584	2.4

Table S3 shows the variation of vibrational frequencies between the free pyridine and the various HCMDC-Py complexes. All the vibrational frequencies of the HCMDC-Py complexes in this table show blue shifts with respect to fundamental frequencies of the free pyridine molecule. The extent of the frequency shift depends on the binding interaction between the pyridine molecule and the metal cluster. From the table, it can be seen that the vibrational frequency shift of ν_{6a} mode is very sensitive to the bonding sites. For the complexes of the pyridine molecule adsorbed on the Au-Cu HCMDC, the frequency of ν_{6a} mode increases from 613 cm^{-1} in the Cu-Au-Py to 635 cm^{-1} in the Au-Cu-Py.

4. Raman vibrational analysis of HCMDC-Py complexes at 785 nm, 514 nm,

and 488 nm excitations.

Table S4. Raman vibrational peaks (wave number in cm^{-1}) and DRCS (in units of $10^{-30}cm^2/sr$) of selected totally symmetric modes of the HCMDC-Py complexes under a C_{2v} point group calculated using the B3LYP method at 785 nm, 514 nm, and 488 nm excitation light (EX in units of nm).

		υ_{6a}		υ_1		υ_{12}		υ_{9a}		υ_{8a}	
	EX	peak	dσ/dΩ	peak	dσ/dΩ	peak	dσ/dΩ	peak	dσ/dΩ	peak	dσ/dΩ
	785	613	0.03	991	2.3	1016	2.7	1196	0.5	1584	2
Ag-Au-Py	514	613	0.4	991	4	1016	12	1196	3	1584	7
	488	613	1.2	991	5.7	1016	17	1196	5.5	1584	12.7
	785	619	0	996	1.5	1021	1.3	1204	0.2	1590	1
Au-Ag-Py	514	619	0.4	996	2.8	1021	4	1204	1	1590	3.4
	488	619	66613	996	5576	1021	26653	1204	0.1	1590	35406
	785	615	0	993	1.6	1017	1.5	1201	0.3	1585	1.2
Cu-Ag-Py	514	615	1.1	993	3	1017	11	1201	2	1585	7.6
	488	615	6	993	3	1017	22	1201	3.3	1585	12
	785	628	1	998	7	1023	0	1199	2	1590	11
Ag-Cu-Py	514	628	1	998	27	1023	2	1199	21	1590	89
	488	628	1.7	998	40	1023	3.8	1199	40	1590	157
	785	635	1	1001	8	1028	0	1200	2	1592	12
Au-Cu-Py	514	635	4	1001	52	1028	0.2	1200	46	1592	139
	488	635	3.6	1001	49	1028	0.2	1200	42	1592	146
	785	613	0.1	991	3	1016	2	1196	1	1584	3
Cu-Au-Py	514	613	0.6	991	8	1016	21	1196	7	1584	19
	488	613	10	991	2	1016	45	1196	10	1584	21

5. The complete author list of reference 23.

The complete author list of reference 23 is provided as following:

Frisch, M. J.; Trucks, G. W.; Schlegel, H. B.; Scuseria, G. E.; Robb, M. A.; Cheeseman, J. R.; Montgomery, Jr., J. A.; Vreven, T.; Kudin, K. N.; Burant, J. C.; Millam, J. M.; Iyengar, S. S.; Tomasi, J.; Barone, V.; Mennucci, B.; Cossi, M.; Scalmani, G.; Rega, N.; Petersson, G. A.; Nakatsuji, H.; Hada, M.; Ehara, M.; Toyota, K.; Fukuda, R.; Hasegawa, J.; Ishida, M.; Nakajima, T.; Honda, Y.; Kitao, O.; Nakai, H.; Klene, M.; Li, X.; Knox, J. E.; Hratchian, H. P.; Cross, J. B.; Bakken, V.; Adamo, C.; Jaramillo, J.; Gomperts, R.; Stratmann, R. E.; Yazyev, O.; Austin, A. J.; Cammi, R.; Pomelli, C.; Ochterski, J. W.; Ayala, P. Y.; Morokuma, K.; Voth, G. A.; Salvador, P.; Dannenberg, J. J.; Zakrzewski, V. G.; Dapprich, S.; Daniels, A. D.; Strain, M. C.; Farkas, O.; Malick, D. K.; Rabuck, A. D.; Raghavachari, K.; Foresman, J. B.; Ortiz, J.

V.; Cui, Q.; Baboul, A. G.; Clifford, S.; Cioslowski, J.; Stefanov, B. B.; Liu, G.; Liashenko, A.; Piskorz, P.; Komaromi, I.; Martin, R. L.; Fox, D. J.; Keith, T.; Al-Laham, M. A.; Peng, C. Y.; Nanayakkara, A.; Challacombe, M.; Gill, P. M. W.; Johnson, B.; Chen, W.; Wong, M. W.; Gonzalez, C.; Pople, J. A. GAUSSIAN03, revision D.01. Gaussian Inc.: Wallingford. 2004.